that the Si–O bond lengths within the silicon oxygen ring are larger than the peripheral bonds Si_1–O_1, Si_2–O_2 and Si_2–O_4 in crocidolite and actinolite. This is not true, however, in the case of cummingtonite.

Table 7. *Interatomic bond angles in cummingtonite*

Si–O–Si	
Si_1–O_5–Si_2	142·9°, 139·4°
Si_1–O_6–Si_2	141·4
Si_1–O_7–Si_1	142·2
Mean	141·5°
O–Si_1–O	
O_7–Si_1–O_1	110·5°
O_6–Si_1–O_1	109·9
O_5–Si_1–O_1	109·8
O_7–Si_1–O_6	108·8
O_6–Si_1–O_5	109·3
O_5–Si_1–O_7	108·6
Mean	109·5°
O–Si_2–O	
O_4–Si_2–O_2	116·3°
O_5–Si_2–O_2	109·0
O_6–Si_2–O_2	107·7
O_5–Si_2–O_6	110·3
O_6–Si_2–O_4	104·7
O_4–Si_2–O_5	109·0
Mean	109·5°

Though the silicon–oxygen distances within two Si–O tetrahedra are not significantly different, the O–Si–O bond angles show that the Si_1–O tetrahedron is more regular, in which O–Si_1–O bond angles range from 108·6° to 110·5°, while O–Si_2–O bond angles range from 104·7° (O_6–Si_2–O_4) to 116·3° (O_4–Si_2–O_2). It may be noted that the two distorted tetrahedral angles in the Si_2–O tetrahedron involve O_4. The distortion in the Si_2–O tetrahedron, therefore, is certainly caused by the strong attraction between O_4 and M_4.

The closest approach between oxygen atoms in two neighboring silicate chains is 2·97 Å. This distance is very comparable to those in crocidolite and actinolite, which are 2·97 and 2·9 Å.

The author is greatly indebted to Prof. Erwin E. Hellner for technical assistance and valuable discussions. He is grateful to Prof. Hans Ramberg for his interest and to Prof. George A. Jeffrey for the use of the University of Pittsburgh computation facilities, with the support of a grant from the National Science Foundation. The financial assistance from the University of Chicago in the form of fellowships and grants to cover the cost of the earlier part of the computations is gratefully acknowledged.

References

Berghuis, J., Haanappel, IJ. M., Potters, M., Loopstra, B. O., MacGillavry, C. H. & Veenendaal, A. L. (1955). *Acta Cryst.* **8**, 478.
Bommel, A. J. van, & Bijvoet, J. M. (1958). *Acta Cryst.* **11**, 61.
Busing, W. R. & Levy, H. A. (1959). Oak Ridge National Laboratory, Central Files Number 59-4-37.
Flaschen, S. S. & Osborn, E. F. (1957). *Econ. Geol.* **52**, 923.
Freeman, A. J. (1959). *Acta Cryst.* **12**, 271.
Ghose, S. & Hellner, E. (1959). *J. Geol.* **67**, 691.
Heritsch, H., Paulitsch, P. & Walitzi, E. M. (1957). *Tsch. Min. Pet. Mitt.* **6**, 215.
Mueller, R. F. (1960). *Amer. J. Sci.* **258**, 449.
Senko, M. E. & Templeton (1957). *Acta Cryst.* **10**, 385.
Warren, B. E. (1930). *Z. Kristallogr.* **72**, 42.
Whittaker, E. J. W. (1949). *Acta Cryst.* **2**, 312.
Zalkin, A. & Jones, R. E. (1957). *Acta Cryst.* **10**, 385.
Zussman, J. (1955). *Acta Cryst.* **8**, 385.
Zussman, J. (1959). *Acta Cryst.* **12**, 309.

Acta Cryst. (1961). **14**, 627

A Theoretical Study of Pendellösung Fringes. Part 2. Detailed Discussion Based upon a Spherical Wave Theory

By N. Kato

Division of Engineering and Applied Physics, Harvard University, Cambridge, Massachusetts, U.S.A.

(*Received* 19 *May* 1960)

Based upon the general formulation of Part 1, explicit expressions for the crystal wave fields and the vacuum wave fields are obtained assuming a spherical wave as the incident beam. For thick parts of crystals, absorption effects are taken into account. The same results as expected from the energy-flow theory (Kato, 1960) are obtained as a special case. 'Pendellösung' phenomena of X-rays are discussed. In particular, 'hook-shaped' patterns (Kato & Lang, 1959) can be fully explained. Values of integrated intensity according to the ordinary theory do not need to be revised.

1. Introduction

In Part 1 (Kato, 1960), we arrived at the conclusion that single-crystal diffraction in X-ray cases falls under a category in which (*a*) a spherical wave approximation is more appropriate, yet at the same time (*b*) the curvature of the wave surface of the incident

wave can be neglected. Following this conclusion, a theory has been developed assuming a spherical wave as the incident wave. We will call it spherical-wave theory, in contrast to the ordinary theory which may be called plane-wave theory. This development was necessary for understanding 'Pendellösung' phenomena in X-rays. It is also of interest because in certain respects the theory is an extreme alternative to the plane-wave theory.

The problem is essentially that of evaluating wave fields in an explicit form based upon the equations from (19) to (22) of Part 1. A steepest-descent method is applicable for this purpose. In our problem, however, this approach is not perfectly satisfactory because the dispersion surface has an unusual form. The method is useful only for the relatively thick parts of a crystal. If the condition (*b*) is satisfied, however, the required definite integrals for the non-absorption case can be evaluated directly. Thus we can obtain wave fields for almost all cases of practical interest.

With respect to the intensity distribution of the transmitted and the reflected beam averaged over the 'Pendellösung' periodicity, the results are compared with the energy-flow theory (Laue, 1952; Kato, 1960). 'Pendellösung' phenomena are discussed and comparison made with the theory developed in electron cases. Both energy flow and electron theory are based upon the plane-wave assumption, but hook-shaped patterns (Kato & Lang, 1959) are understandable only in terms of the present theory. In connection with traverse patterns, integrated intensities are also discussed and are shown to be the same as those given by the plane-wave theory.

2. Crystal wave fields

We start from equations (1–19)* and (1–20) using $F_s(\hat{\mathbf{K}})$ of equations (1–9) in place of $F(\hat{\mathbf{K}})$. Thus we obtain crystal wave fields as follows:

Transmitted wave:

$$\varphi_0^{(j)}=\frac{i}{8\pi^2K}\iint_{-\infty}^{+\infty}\frac{C_0^{(j)}}{\cos(\mathbf{K}_A\mathbf{z})}\exp iT^{(j)}dK_xdK_y\,. \tag{1}$$

Diffracted wave

$$\varphi_g^{(j)}=\frac{i\exp 2\pi i(\mathbf{g}\cdot\mathbf{r})}{8\pi^2K}\iint_{-\infty}^{+\infty}\frac{C_g^{(j)}}{\cos(\mathbf{K}_A\mathbf{z})}\exp iT^{(j)}dK_xdK_y\,, \tag{2}$$

where

$$T^{(j)}=(\mathbf{K}\cdot\mathbf{r}_e)+\{\mathbf{k}^{(j)}\cdot(\mathbf{r}-\mathbf{r}_e)\}\,. \tag{3}$$

The vector $\mathbf{r}$ is the position vector of the point of observation, and $\mathbf{r}_e$ specifies a point on the incident surface. Wave vectors $\mathbf{K}$ and $\mathbf{k}^{(j)}$ are connected by a tangential continuity relation expressed by

$$\mathbf{k}^{(j)}=\mathbf{K}+\mathbf{n}A^{(j)}, \tag{4}$$

where $\mathbf{n}$ is an inwardly directed normal of the incident surface and $A^{(j)}$ are given by equations following (see equation (7)).

For convenience choose rectangular coordinate axes in reciprocal space with the origin at the Laue point, L. The y-axis is perpendicular to a plane defined by the reciprocal-lattice vector $\mathbf{g}$ and a radius vector $\mathbf{r}$. The x-axis is the tangent to the wave surface $|\mathbf{K}|=K$ at the Laue point*. Hence the z-axis has the direction of the wave vector $\mathbf{K}$ which satisfies the Bragg condition exactly. Call such a wave vector $\mathbf{K}_B$.

In real space we use x-, y-, z-axes having the same directions. However, we fix their origin at the light source.

Let us introduce the parameter

$$s=S-\frac{K}{2\sin 2\theta_B}\left(\frac{\gamma_g}{\gamma_0}-1\right)\psi_0^r \tag{5}$$

where S is the x-coordinate of the wave point of a plane wave in vacuum, so that

$$S=-K_x\,. \tag{6}$$

The angle θ_B is the Bragg angle, γ_0 and γ_g stand for $\cos(\mathbf{n}_A\mathbf{K}_B)$ and $\cos(\mathbf{n}_A\mathbf{K}_B+2\pi\mathbf{g})$ respectively. ψ_0^r is the real part of ψ_0, the mean polarizability of the crystal. Superscripts r and i are used for specifying the real and the imaginary parts of a quantity.

$A^{(j)}$, $C_0^{(j)}$ and $C_g^{(j)}$ in equations (1), (2) and (4) can be expressed in terms of s as follows, on the basis of the dispersion relation given by (1–17)

$$A^{(j)}=A^r+iA^i \tag{7}$$

$$A^r=\frac{K}{2\gamma_0}\psi_0^r+\alpha\{s\pm(s^2+\beta^2)^{\frac{1}{2}}\} \tag{8}$$

$$A^i=\frac{K}{4}\psi_0^i\left(\frac{1}{\gamma_0}+\frac{1}{\gamma_g}\right)\pm\frac{K}{4}\psi_0^i\left(\frac{1}{\gamma_g}-\frac{1}{\gamma_0}\right)\frac{s}{(s^2+\beta^2)^{\frac{1}{2}}}\pm\frac{\alpha\beta^2\chi}{(s^2+\beta^2)^{\frac{1}{2}}} \tag{9}$$

$$C_0^{(j)}=\frac{\mp s+(s^2+\beta^2)^{\frac{1}{2}}}{2(s^2+\beta^2)^{\frac{1}{2}}} \tag{10}$$

$$C_g^{(j)}=\frac{1}{2}\left(\frac{\gamma_0}{\gamma_g}\right)^{\frac{1}{2}}\beta\exp[i\delta]\frac{\pm 1}{(s^2+\beta^2)^{\frac{1}{2}}}\,. \tag{11}$$

In these formulae, the upper sign corresponds to the (1) branch of the dispersion surface and the lower sign corresponds to the (2) branch, respectively. For simplicity, the superscripts (j) in A^r and A^i are omitted. $\chi=\psi_g^i/\psi_g^r$, where ψ_g is the $\mathbf{g}$th order Fourier coefficient of the polarizability, and δ is the phase angle of the ψ_g^r. $\sin\chi$ is the polarization factor, 1 and $\cos 2\theta_B$ for parallel and normal polarization respectively. In addition,

* The equations of Part 1 are referred to as (1–19); equations of the paper on energy flow (Kato, 1960) are referred to as (E–3).

* In this paper, the direction of x-axis is taken in the opposite direction of that shown in Fig. 1 of the previous paper (part 1).

$$\alpha = \sin 2\theta_B/(2\gamma_g) \tag{12}$$

and

$$\beta = K|\psi_g^r| \sin\chi/(\gamma_g/\gamma_0)/(\sin 2\theta_B)\ . \tag{13}$$

The procedure for deriving equations (7)–(11) is essentially the same as that described in standard texts (for example, Zachariasen, 1945). Two remarks may be added. Firstly, s is related to Zachariasen's symbol y by

$$s = -\beta y\ . \tag{14}$$

Secondly, we choose here the form $\exp iKr/(4\pi r)$ as the expression for an outgoing wave. Therefore, the signs of ψ_0^i and χ should be changed if we compare A^i with the corresponding expressions in Zachariasen's book.

3. Steepest-descent approximation

Equations (1) and (2) have a typical form to which a steepest descent method is applicable (for example, Jeffreys & Jeffreys, 1946). Thus, the wave fields can be expressed approximately as follows:

$$\varphi_0^{(j)} = i \exp i\{-\tfrac{1}{4}\pi \pm \tfrac{1}{4}\pi\}/(4\pi K)\cdot [C_0^{(j)}/\cos(K\wedge z)]_0^* \times \exp i[T^{(j)}]^*/[|T_{xx}^{(j)}|^{\frac{1}{2}}]_0^* [|T_{yy}^{(j)}|^{\frac{1}{2}}]_0^* \tag{15a}$$

$$\varphi_g^{(j)} = i \exp i\{-\tfrac{1}{4}\pi \pm \tfrac{1}{4}\pi\}/(4\pi K)\cdot [C_g^{(j)}/\cos(K\wedge z)]_0^* \times \exp i[T^{(j)}]^* \exp 2\pi i(\mathbf{g}\cdot\mathbf{r})/[|T_{xx}^{(j)}|^{\frac{1}{2}}]_0^* [|T_{yy}^{(j)}|^{\frac{1}{2}}]_0^*, \tag{15b}$$

where $[\ ]^*$ denotes the value at a saddle point and $[\ ]_0^*$ denotes the corresponding value at a saddle point neglecting absorption effects. $T_{xx}^{(j)}$ and $T_{yy}^{(j)}$ are the second derivatives of $T^{(j)}$ with respect to K_x and K_y.

Equations (15a) and (15b) hold only when the higher terms in the Taylor expansion of $T^{(j)}$ are sufficiently small compared with the second terms in the range of K_x and K_y where $\frac{1}{2}\{T_{xx}K_x^2\} \lesssim 1$ and $\frac{1}{2}\{T_{yy}K_y^2\} \lesssim 1$. This condition does not cause any trouble in performing the integration of K_y provided that K is sufficiently large. In the integration of K_x, we have to be more careful. First of all, unless either

$$|\partial^2(\mathbf{K}\cdot\mathbf{r})/\partial K_x^2| \ll |\partial^2 A^r/\partial K_x^2| t_0 \tag{16}$$

or the reverse condition is satisfied, $T_{xx}^{(j)}$ is approximately zero. Here t_0 stands for $\{\mathbf{n}\cdot(\mathbf{r}-\mathbf{r}_e)\}$ which is the distance between an observation point and the incident surface. The difficulty arises because the curvature of the wave surface $|\mathbf{K}| = K$ and the (1) branch of the dispersion surface are opposite to each other. Thus, the higher terms cannot be neglected. It should be noticed that condition (16) is equivalent to the condition (b) described in Section 1.

Secondly, if A^r is not to be neglected in equation (4), i.e. we are near a Bragg reflection, another condition on the thickness t_0 should be satisfied. The necessary condition in our particular case can be written

$$2\sqrt{2}|A_{xxx}^r|/3 < |A_{xx}^r|^{\frac{3}{2}} t_0^{\frac{1}{2}}\ , \tag{17}$$

where the subscript x means a derivative with respect to K_x.

(a) *Non-Bragg reflection cases*

We assume that the reverse condition of equation (16) is sufficiently well satisfied. This case is not important from the viewpoint of diffraction. Consideration of it, however, illustrates applicability of the present method, particularly for the transmitted beam.

Saddle points are found by a simple calculation to be

$$\begin{cases} x + \dfrac{\partial K_z}{\partial K_x} z = 0 \\ \dfrac{\partial K_z}{\partial K_y} z = 0\ , \end{cases}$$

which gives

$$[K_x/K_z]^* = x/z \tag{18a}$$

and

$$[K_y]^* = 0\ . \tag{18b}$$

Consequently, we have

$$[(\mathbf{K}\cdot\mathbf{r})]^* = Kr\ . \tag{19}$$

In addition, we can write

$$[T_{xx}^{(j)}]^* = -\frac{(r/K)}{[\cos^2(\mathbf{K}\wedge z)]^*} \tag{20a}$$

and

$$[T_{yy}^{(j)}]^* = -(r/K)\ . \tag{20b}$$

In this case, both of $C_g^{(j)}$ and one of $C_0^{(j)}$ are equal to zero and the other $C_0^{(j)}$ is 1. For the last-named (j), $A^{(j)}$ tends to $\frac{1}{2}K\psi_0/\gamma_0$. Thus, from equation (15a),

$$\varphi_0^{(1)} + \varphi_0^{(2)} = \frac{1}{4\pi r} \exp\{iKr + \tfrac{1}{2}iK\psi_0 t_0/\gamma_0\}\ . \tag{21}$$

This is the expected result since we assumed a spherical wave as an incident wave.

(b) *Bragg reflection cases*

The integration K_y can be carried out just as described in case (a), since $A^{(j)}$ does not include K_y. In this section, we assume t_0 to be large enough to satisfy the conditions (16) and (17). Therefore, we are concerned with a fairly thick crystal in which absorption may not be neglected. In performing the integration of K_x, however, we start first from a non-absorbing crystal. From equations (3), (4), (5) and (6), neglecting terms higher than the second in the Taylor expansion of $(\mathbf{K}\cdot\mathbf{r})$ around the Laue point, we may write $T^{(j)} = (\mathbf{K}\cdot\mathbf{r}) + A^{(j)}\{\mathbf{n}\cdot(\mathbf{r}-\mathbf{r}_e)\}$ as follows:

$$T^{(j)} \simeq (Kz) + P - [sq \mp \alpha(s^2+\beta^2)^{\frac{1}{2}}]t_0\ , \tag{22}$$

where

$$P = \frac{K\psi_0^r}{2\sin 2\theta_B}\left(\frac{\gamma_g}{\gamma_0} - 1\right)x + \frac{K\psi_0^r}{2\gamma_0} t_0 \tag{23}$$

and

$$q = (x - \alpha t_0)/t_0\ . \tag{24}$$

Throughout these expressions x and z are used for $\mathbf{x}$- and $\mathbf{z}$-coordinates of the radius vector $\mathbf{r}$.

The saddle-point condition, $\partial T^{(j)}/\partial K_x=0$, gives

$$[s/(s^2+\beta^2)^{\frac{1}{2}}]_0^*=\pm q/\alpha\,. \tag{25}$$

If we write

$$X=\pm q/\alpha \tag{26}$$

the parameter X is exactly the same as that given by equation (E–3), since equation (14) holds. Given $\mathbf{r}$ and consequently q, we can determine the parameters $[s]_0^*$ and X. It should be noticed that the parameters $[s]_0^*$ and X corresponding to the same observation point but to the different branches of the dispersion surface have opposite signs. We call such saddle points conjugate.

If we denote by $\mathbf{R}_e$ a radius vector $\mathbf{r}_e$ which is parallel to the vector $\mathbf{K}_B$, we can write $T^{(j)}$ as

$$T^{(j)}=(\mathbf{K}\cdot\mathbf{R}_e)+\{\mathbf{k}^{(j)}\cdot(\mathbf{r}-\mathbf{R}_e)\}\,. \tag{27}$$

By the same approximation used in deriving (22), the saddle-point condition gives

$$\delta T^{(j)}\simeq\{\delta\mathbf{k}^{(j)}\cdot(\mathbf{r}-\mathbf{R}_e)\}=0\,. \tag{28}$$

This means that we may substitute

$$\mathbf{r}-\mathbf{R}_e=\nu l\,, \tag{29}$$

where the direction ν is the normal of the dispersion surface at the saddle point. Thus

$$T^{(j)}=(KL)+(\mathbf{k}^{(j)}.\nu)l \tag{30}$$

in which L is the magnitude of $\mathbf{R}_e$. Then through equation (25) $\mathbf{k}^{(j)}$ and $T_{xx}^{(j)}$ may be expressed as functions of the observation point.

Next we consider absorption effects. In absorbing crystals, the saddle points cannot be determined on the real axis of K_x, because the quantities $A^{(j)}$ include an imaginary part. Since A^i is not very large, however, we can use the saddle points for non-absorbing cases as first approximation. Actually, we take into account absorption effects only when evaluating the phase term $[T^{(j)}]^*$, as has been assumed already in equation (15).†

$$T^{(j)}=[T]_0^*+\left[\frac{\partial T}{\partial K_x}\right]_0^*(u+iv)+\tfrac{1}{2}\left[\frac{\partial^2 T}{\partial K_x^2}\right]_0^*(u+iv)^2+\ldots \tag{31}$$

in which

$$u+iv=K_x-[K_x]_0^*\,. \tag{32}$$

Therefore the saddle points are given by the condition

$$\partial T/\partial K_x=i[\partial A^i/\partial K_x]_0^*t_0+[\partial^2 A/\partial K_x^2]_0^*t_0(u+iv)=0 \tag{33}$$

since $[\partial T^r/\partial K_x]_0^*=0$ and $(\partial^2 K_z/\partial K_x^2)z$ can be neglected.

Taking the real and imaginary part of equation (33), u and v may be determined easily. Thus, it turns out that

$$[T]^*=[T]_0^*+\Delta_a T, \tag{34}$$

where $\Delta_a T$ is given by

$$\Delta_a T=\frac{1}{2}\left[\frac{\left(\frac{\partial A^i}{\partial K_x}\right)^2\left(\frac{\partial^2 A^r}{\partial K_x^2}\right)}{\left(\frac{\partial^2 A^r}{\partial K_x^2}\right)^2+\left(\frac{\partial^2 A^i}{\partial K_x^2}\right)^2}\right]_0^* t_0-\frac{i}{2}\left[\frac{\left(\frac{\partial A^i}{\partial K_x}\right)^2\left(\frac{\partial^2 A^i}{\partial K_x^2}\right)}{\left(\frac{\partial^2 A^r}{\partial K_x^2}\right)^2+\left(\frac{\partial^2 A^i}{\partial K_x^2}\right)^2}\right]_0^* \tag{35}$$

Quantities involved here can be evaluated by differentiation of equations (8) and (9). In order to estimate the magnitude of $\Delta_a T$ we consider a symmetrical Laue case: $\gamma_0=\gamma_g$. In this case it turns out that

$$\Delta_a T=\simeq\pm\tfrac{1}{2}f_1(s)\chi^2\alpha\beta t_0\pm\tfrac{1}{2}f_2(s)\chi^3\alpha\beta t_0 i\,, \tag{36}$$

where f_1 and f_2 are less than 1 and they tend to zero for both the extreme cases in which s tends either to zero or to $\pm\infty$.† Thus we see that we can neglect correction terms for absorption under the usual experimental conditions where $\chi<0{\cdot}1$.

Using the above results we finally obtain the crystal wave fields as

$$\varphi_0^{(1)}=(i/8\pi)(1/t_0 r)^{\frac{1}{2}}(\beta/K\alpha)^{\frac{1}{2}}(1+X)/(1-X^2)^{\frac{3}{4}}\times\exp iKL.\exp i(\mathbf{k}\cdot\nu)l.\exp -A^i t_0 \tag{37a}$$

$$\varphi_0^{(2)}=(1/8\pi)(1/t_0 r)^{\frac{1}{2}}(\beta/K\alpha)^{\frac{1}{2}}(1-X)/(1-X^2)^{\frac{3}{4}}\times\exp iKL.\exp i(\bar{\mathbf{k}}\cdot\nu)l.\exp -\bar{A}^i t_0 \tag{37b}$$

$$\varphi_g^{(1)}=(i/8\pi)(1/t_0 r)^{\frac{1}{2}}(\beta/K\alpha)^{\frac{1}{2}}(\gamma_0/\gamma_g)^{\frac{1}{2}}\times\exp i\{\delta+2\pi(\mathbf{g}\cdot\mathbf{r})\}/(1-X^2)^{\frac{1}{4}}\times\exp iKL.\exp i(\mathbf{k}\cdot\nu)l\exp -A^i t_0 \tag{38a}$$

$$\varphi_g^{(2)}=(-1/8\pi)(1/t_0 r)^{\frac{1}{2}}(\beta/K\alpha)^{\frac{1}{2}}(\gamma_0/\gamma_g)^{\frac{1}{2}}\times\exp i\{\delta+2\pi(\mathbf{g}\cdot\mathbf{r})\}/(1-X^2)^{\frac{1}{4}}\times\exp iKL.\exp i(\bar{\mathbf{k}}\cdot\nu)l\exp -\bar{A}^i t_0\,. \tag{38b}$$

Here we use $\mathbf{k}$ and A^i for $k^{(1)}$ and $A^{(1)i}$ and also $\bar{\mathbf{k}}$ and $\bar{A}^i$ instead of $\mathbf{k}^{(2)}$ and $A^{(2)i}$ in order to emphasize that they correspond to conjugate points.

4. Wave field of non-absorbing crystals

Under usual experimental conditions, roughly speaking, the critical thicknesses are a few tenths of a mm. to satisfy condition (17) and of order 10μ to satisfy condition (16) along the direction $q=0$. On the other hand, fringe distances are of order 50μ. Thus, it is very necessary to obtain a more rigorous expression for wave fields in the thin crystal case. In this section we assume only the condition (16), and we neglect absorption.

Substituting for $C_0^{(j)}$, $C_g^{(j)}$ and $T^{(j)}$ from equations (10), (11) and (22) in equations (1) and (2), $\Sigma\varphi_0^{(j)}$ and $\Sigma\varphi_g^{(j)}$ can be integrated directly (Appendix A). The results are as follows, when $|q|<\alpha$,

† Here we have omitted the superscript (j), and we will do so when no confusion is likely.

† In asymmetrical cases, $\gamma_0\neq\gamma_g$, f_1 and f_2 do not tend to zero in the case $s=0$.

$$\Sigma\varphi_0^{(j)}=(-i/4\sqrt{2\pi})(1/Kr)^{\frac{1}{2}} \times\exp i\{-\tfrac{1}{4}\pi+(Kz)+P\} \times\beta((\alpha-q)/(\alpha+q))^{\frac{1}{2}}J_1(\zeta) \quad (39a)$$

$$\Sigma\varphi_g^{(j)}=(-1/4\sqrt{(2\pi)})(1/Kr)^{\frac{1}{2}} \times\exp i\{-\tfrac{1}{4}\pi+(Kz)+P+2\pi(\mathbf{g}\cdot\mathbf{r})\} \times(K\psi_g\sin\chi/\sin 2\theta_B).J_0(\zeta)\,. \quad (39b)$$

In these expressions

$$\zeta=t_0\beta(\alpha^2-q^2)^{\frac{1}{2}} \quad (40)$$

and J_0 and J_1 are the zeroth and the first-order Bessel functions, respectively.

When $|q|>\alpha$ we find

$$\Sigma\varphi_0^{(j)}=0 \quad (39c)$$

$$\Sigma\varphi_g^{(j)}=0\,. \quad (39d)$$

These equations imply that the wave fields are limited to the area between directions $\mathbf{K}_B$ and $\mathbf{K}_B+2\pi\mathbf{g}$ which pass through a point $\mathbf{R}_e$ (see Fig. 1). We shall return to this point again in Section 7.

Expressions (39*a*, *b*) should tend to expressions (37*a*, *b*) and (38*a*, *b*) neglecting absorption and increasing the distance t_0. This can be shown to be so using the following asymptotic formulae for J_0 and J_1 for large arguments.

$$J_0(\zeta)=(2/\pi\zeta)^{\frac{1}{2}}\cos(\zeta-\tfrac{1}{4}\pi)$$
$$J_1(\zeta)=(2/\pi\zeta)^{\frac{1}{2}}\cos(\zeta+\tfrac{3}{4}\pi)\,.$$

When the cosine is expressed by exponential terms, each term corresponds to either the (1) or the (2) wave of equations (37*a*, *b*) and (38*a*, *b*).

5. Vacuum wave fields

Vacuum wave fields near the crystal can be expressed by equations (1–21) and (1–22). These are evaluated by procedures similar to those described in Section 3 and Section 4. It is, however, much more convenient to express the vacuum waves in terms of crystal waves described above. In the case of the transmitted beam, the phase is expressed as

$$T_0^{(j)}=\{(\mathbf{K}-\mathbf{k}_0^{(j)})\cdot\mathbf{r}_e\}+\{(\mathbf{k}_0^{(j)}-\mathbf{K}_0)\cdot\mathbf{r}_a\}+(\mathbf{K}_0\cdot\mathbf{r}) =T^{(j)}(\mathbf{r}_a)+\{\mathbf{K}_0\cdot(\mathbf{r}-\mathbf{r}_a)\}\,. \quad (41)$$

Since $\mathbf{r}_a$ is an arbitrary vector on the exit surface, we can specify it for a given $\mathbf{r}$ so that we have

$$\mathbf{r}-\mathbf{R}_a^0\,||\,\mathbf{K}_B\,, \quad (42)$$

where $\mathbf{R}_a^0$ stands for such a specified vector $\mathbf{r}_a$. Neglecting the curvature of the wave surface $|\mathbf{K}_0|=K$, $\{\mathbf{K}_0\cdot(\mathbf{r}-\mathbf{R}_a^0)\}\simeq KL^0$ where

$$L^0=|\mathbf{r}-\mathbf{R}_a^0|\,, \quad (43)$$

if L^0 is not too large.

Therefore, we can write the wave fields at $\mathbf{r}$ in vacuum as

$$\Phi_0(\mathbf{r})=\exp iKL^0\sum_j\varphi_0^{(j)}(\mathbf{R}_a^0)\,. \quad (44)$$

Similarly, in the case of the reflected beam

$$\Phi_g(\mathbf{r})=\exp iKL^g\sum_j\varphi_g^{(j)}(\mathbf{R}_a^g)\,, \quad (45)$$

where we have

$$\mathbf{r}-\mathbf{R}_a^g\,||\,\mathbf{K}_B+2\pi\mathbf{g} \quad (46)$$

and

$$L^g=|\mathbf{r}-\mathbf{R}_a^g|\,. \quad (47)$$

Thus, the intensity distributions over the cross sections of the transmitted and reflected beams are given by

$$I_0(\mathbf{r})=(c/8\pi)\Big|\sum_j\varphi_0^{(j)}(\mathbf{R}_a^0)\Big|^2 \quad (48)$$

$$I_g(\mathbf{r})=(c/8\pi)\Big|\sum_j\varphi_g^{(j)}(\mathbf{R}_a^g)\Big|^2\,. \quad (49)$$

Comparison with the energy-flow theory

Assuming converging plane waves with no phase relation between them, we expect intensity distributions across the diffracted and the transmitted beams as obtained in a previous paper (Kato, 1960). There we assumed that the energy which flows through an angular range $(\delta s/K)$ is

$$I_e\delta y=I_e(K/\beta)(\delta s/K)\,,$$

where y is given by equation (14). In the present treatment we assume a spherical wave $1/(4\pi r)\exp iKr$ as the incident wave. This implies that the energy which flows through an angular range $(\delta s/K)$ at a point $\mathbf{r}$ is

$$(c/8\pi)(1/4\pi r)^2.r(\delta s/K)\,.$$

In order to compare the theories we equate the above expressions. Thus, we obtain

$$I_e=c\beta/(128\pi^3 rK)\,. \quad (50)$$

In thick crystals we may derive the intensity formulae by inserting equations (37) and (38) into equations (48) and (49). Similar formulae are also obtained from equations (E–10) and (E–11) based upon the energy-flow theory. In these formulae $|dX/dp|(\delta p/\delta\xi)$ and $|dX/dp|(\delta p/\delta\eta)$ are given by equations (E–B3*a*) and (E–B3*b*). Thus, it turns out that equations (E–10) and (E–11) become

$$I_0(\xi)=I_e/(4t_0\alpha)\cdot 1/(1-X^2)^{\frac{1}{2}} \times\{(1+X)/(1-X)\cdot\exp -2A^it_0 +(1-X)/(1+X)\cdot\exp -2\bar{A}^it_0\}$$

$$I_g(\eta)=I_e/(4t_0\alpha)\cdot 1/(1-X^2)^{\frac{1}{2}} \times\{\exp[-2A^it_0]+\exp[-2\bar{A}^it_0]\}$$

using the notations α, A^i and $\bar{A}^i$ of the present paper. These equations are exactly the same as the intensity formulae based upon the spherical wave theory if we average the latter over the Pendellösung period.

In a region where equations (39*a*) and (39*b*) should be used instead of equations (37) and (38), the distributions are different from what is expected from the simple energy-flow theory. However, we expect a similar intensity enhancement at the margins of the diffracted beam. This is easily concluded from the form of the Bessel function J_0.

6. Pendellösung interference

(*a*) *Section patterns*

It is convenient to consider the intensity field† in a crystal. The section patterns are given by the cross section of this IF with the exit surface of the crystal as shown in Fig. 3 (see equations (48) and (49)). In a sufficiently deep part of the crystal, we can expect sinusoidal interference between the $\mathbf{k}(\boldsymbol{\nu})$-wave and the $\bar{\mathbf{k}}(\boldsymbol{\nu})$-wave. The fringe spacing along the $\boldsymbol{\nu}$-direction passing through $\mathbf{R}_e$ is given by

$$\Lambda = 2\pi/\{(\mathbf{k}(\boldsymbol{\nu}) - \bar{\mathbf{k}}(\boldsymbol{\nu}))\cdot\boldsymbol{\nu}\} . \tag{51}$$

This has been obtained already by wave bundle considerations in Part 1.

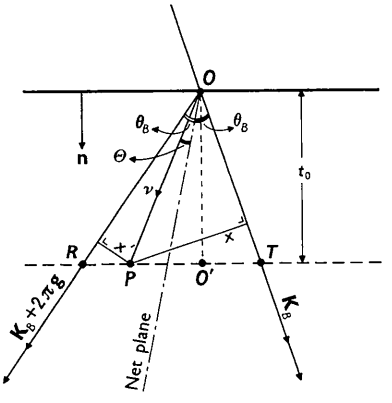

Fig. 1. Geometrical relations between various notations. $TO'=a$, $RO'=b$, $PO'=\tau$.

In the thin crystal region, we cannot describe IF by such a simple interference. Still we can expect interference fringes in IF since $\{J_0\}^2$ and $\{J_1\}^2$ are oscillating functions. The maxima of intensity along a particular direction are determined by values of ζ given by

$$\zeta = \zeta_m^0 \quad \text{and} \quad \zeta_m^1 , \tag{52}$$

where ζ_m^0 and ζ_m^1 are the arguments of successive maximum and minimum points of J_0 and J_1 respectively.

From equations (12) and (24) and Fig. 1

$$\begin{aligned} t_0^2(\alpha^2 - q^2) &= x(2\alpha t_0 - x) \\ &= xx'(\gamma_0/\gamma_g) , \end{aligned}$$

where x and x' indicate the distance from an observation point P to $\mathbf{K}_B$ and $\mathbf{K}_B + 2\pi\mathbf{g}$ respectively as shown in Fig. 1. Therefore, we have

$$\zeta = K|\psi_g^r| \sin\chi/(\sin 2\theta_B)\cdot(xx')^{\frac{1}{2}} . \tag{53}$$

This may also be rewritten as

$$\zeta = K|\psi_g^r| \sin\chi/\sin 2\theta_B \cdot (\gamma_0\gamma_g)^{\frac{1}{2}}((b-\tau)\cdot(\tau-a))^{\frac{1}{2}}, \tag{54}$$

where

$$\tau = PO', \quad a = TO' = t_0 \tan(\mathbf{n}\wedge\mathbf{K}_B) \quad \text{and}$$
$$b = RO' = t_0 \tan(\mathbf{n}\wedge\mathbf{K}_B + 2\pi\mathbf{g})$$

in Fig. 1.

In order to obtain more practical formulae we again rewrite equation (53) using the geometrical parameter

$$p = \tan\Theta/\tan\theta_B ,$$

where Θ means the angle between $\boldsymbol{\nu}$ and the net plane. This is the same as introduced by equation (E–6). Since

$$\begin{aligned} (1/l)(xx')^{\frac{1}{2}} &= \{\sin(\theta_B+\Theta)\sin(\theta_B-\Theta)\}^{\frac{1}{2}} \\ &= \sin\theta_B \cos\Theta\{1-p^2\}^{\frac{1}{2}} \end{aligned}$$

we have

$$\zeta = K|\psi_g^r| \sin\chi/(2\cos\theta_B)\cdot[(1-p^2)/(1+p^2\tan^2\theta_B)]^{\frac{1}{2}} l \tag{55}$$

$$= \Xi(p) l . \tag{56}$$

Equations (53)–(56) show the loci of equal phase in IF. Equation (53) shows directly that these loci are hyperbolae whose asymptotes are $\mathbf{K}_B$ and $\mathbf{K}_B + 2\pi\mathbf{g}$ passing through the point 0 (or $\mathbf{R}_e$). Thus our theory predicts the hook-spaped fringes which are observed in wedge shaped parts of crystals, as already reported (see Fig. 3). If the crystals are parallel-sided we predict a set of parallel fringes. These are also observed as expected. Combining equations (56) and (52) we obtain the loci of intensity maxima and also fringe spacings along the p-direction as follows:

Transmitted beam:

$$\Lambda_{m0} = (\zeta_{m+1}^1 - \zeta_m^1)/\Xi(p) .$$

Reflected beam:

$$\Lambda_{mg} = (\zeta_{m+1}^0 - \zeta_m^0)/\Xi(p) . \tag{57}$$

Since the conjugate wave vectors $\mathbf{k}(\boldsymbol{\nu})$ and $\bar{\mathbf{k}}(\boldsymbol{\nu})$ are specified by s^* and $-s^*$, respectively,

$$\mathbf{k}(\boldsymbol{\nu}) = \mathbf{K}(s^*) + A^{(1)r}(s^*)\mathbf{n}$$

and

$$\bar{\mathbf{k}}(\boldsymbol{\nu}) = \mathbf{K}(-s^*) + A^{(2)r}(-s^*)\mathbf{n} .$$

Then, using equations (24), (25) and (40), we find

$$\{(\mathbf{k}(\boldsymbol{\nu}) - \bar{\mathbf{k}}(\boldsymbol{\nu}))\cdot\boldsymbol{\nu}\}l = 2\{-sx + \alpha t_0(s + (s^2+\beta^2)^{\frac{1}{2}})\}^* = 2\zeta .$$

Comparison with equation (56) shows that

$$\{(\mathbf{k}(\boldsymbol{\nu}) - \bar{\mathbf{k}}(\boldsymbol{\nu}))\cdot\boldsymbol{\nu}\} = 2\Xi(p) . \tag{58}$$

Now, for large m, we have the asymptotic relation that

† We abbreviate this as IF.

$$\zeta_{m+1}^{0}-\zeta_{m}^{0}=\pi$$
$$\zeta_{m+1}^{1}-\zeta_{m}^{1}=\pi\,.$$

Thus equation (51) is an asymptotic form of equation (57).

(*b*) *Traverse patterns*

(i) *Reflected beam.*—In Fig. 2, F indicates a point on the X-ray film. The blackness at F is determined by the total X-rays passing through the corresponding point P on the exit surface, where PF is parallel to $\mathbf{K}_B+2\pi\mathbf{g}$. This total energy is the sum of the X-rays which are excited at the incident surface between A and B, propagate through P, and after that propagate in a direction $\mathbf{K}_B+2\pi\mathbf{g}$. Thus it can be concluded that the blackness at F is proportional to the integrated intensity which would be obtained from a crystal of parallel slab form whose thickness is the distance from P to the incident surface.

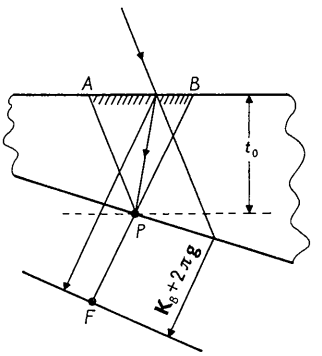

Fig. 2. Contribution of diffracted waves to a point F on X-ray film in the case of traverse patterns.

It is convenient to consider the integrated intensity field (which we will refer to as IIF). Contours of equal integrated intensity are of course parallel to the incident surface. The traverse pattern is given by the section of the IIF cut by the exit surface, in just the same way that it is the section of the IF cut by the exit surface that gives the section pattern.

The integrated intensity R_g is given by

$$R_g=(c/8\pi)\gamma_g\int_T^R|\Sigma\varphi_g^{(j)}(\tau)|^2d\tau\,. \tag{59}$$

The meaning of T, R and τ is shown by Fig. 1. This expression gives the same integrated intensity as that obtained with convergent plane waves which have no phase relation. This is concluded on the basis of Parseval's theorem for Fourier transforms, because the wave fields at the exit surface have the form of the two-dimensional Fourier transform of the wave fields due to the plane-wave theory (see equation (2)). The question arises, however, whether the approximate treatments described above fail to indicate this correspondence. In non-absorbing crystals we can show that the correspondence holds, by integrating equation (59), directly using the expressions (39*b*) and (54). (See Appendix B.) In absorbing cases, it is rather hard to carry out the direct integration of (59) using equation (38*a*, *b*) for $\Sigma\varphi_g^{(j)}(\tau)$. In symmetrical Laue cases, it is possible to show that the above-mentioned correspondence exits. It should be also noticed that the integrated intensities averaged over the 'Pendellösung' period are the same for the plane wave theory and the spherical wave theory, since as mentioned in Section 5 the averaged intensity distribution on the exit surface (see equations (38*a*, *b*)) is the same as that based upon the energy-flow theory.

The integrated intensity for the parallel slab crystal R_g based upon the plane wave theory is given by Waller (1926) for non-absorbing crystals and by Kato (1955) for absorbing crystals. According to them, absorbing affects principally the visibility of the Pendellösung fringes, for if the absorption is low enough to permit observation of Pendellösung fringes at all, its effects on their spacing are insignificant.

'Pendellösung' fringe spacings are determined by Waller's formula

$$R_g=I_e\int_0^{2\alpha\beta t_0}J_0(\varrho)d\varrho\,.$$

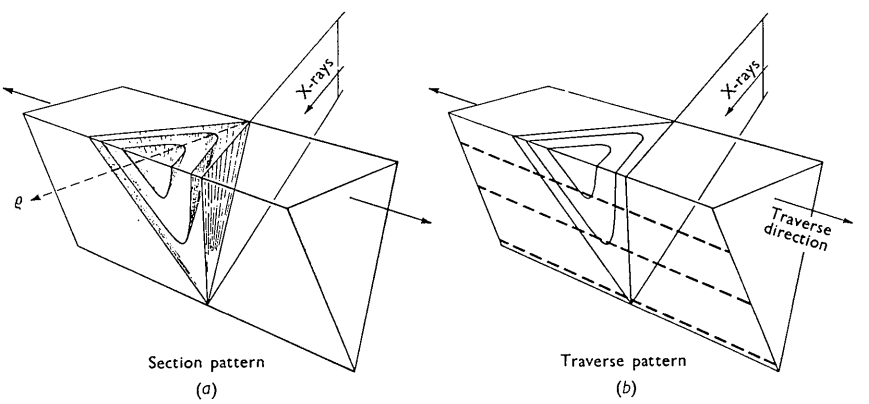

Fig. 3. (*a*) Intensity fields (IF) and section patterns. (*b*) Integrated intensity fields (IIF) and traverse patterns: Dotted lines are fringe maxima.

Therefore the maxima of IIF are given by the condition that

$$\alpha\beta t_0 = \tfrac{1}{2}\varrho_{2m+1} , \qquad (60)$$

where ϱ_{2m+1} is a zero of J_0. Since $\frac{1}{2}\{\varrho_{2m+1}-\varrho_{2m-1}\}$ tends to π for large m the fringes can be approximated by a sinusoidal interference so far as fringe spacings are concerned. Moreover, since $\zeta=\alpha\beta t_0$ along $q=0$ (see equation (40)), fringe spacings of the traverse pattern become equal to those of the section pattern along this direction if the crystal thickness is large enough (see Fig. 3). The traverse pattern of such a crystal is thus determined only by the waves corresponding to $s=0$, i.e., $y=0$. Thus, the tentative approach of the earlier paper (Kato & Lang, 1959) in which fringe distances were calculated in terms of the plane wave theory can be justified approximately for the thick crystal region.

(ii) *Transmitted beam.*—Using the transmitted beam it is difficult to obtain a traverse pattern. Nevertheless, it is of interest to consider the integrated contribution to the transmitted beam due to Bragg reflection, particularly in the non-absorbing case. This contribution may be defined as follows:

$$R_0=(c/8\pi)\gamma_0\int_T^R\{|\Phi_c|^2-|\Phi_s|^2\}d\tau , \qquad (61)$$

where Φ_c stands for complete transmitted waves which are given exactly by equation (1) before integration and Φ_s is a spherical wave given by equation (21). Let us divide the region TR into two regions ε_1 and ε_2, in a rather arbitrary way. The region ε_2 is defined in such a way that for the incident beam propagating towards ε_2 negligible Bragg reflection occurs. In the region ε_1, Bragg reflection cannot be neglected. In the region ε_2, we can write

$$\Phi_c=\Sigma\varphi_0^{(j)}+\Phi_s ,$$

where $\Sigma\varphi_0^{(j)}$ are given by equation (39*a*) for the non-absorbing case. Moreover, we can neglect the interference between the $\varphi_0^{(j)}$ and Φ_s waves since they have very different wave vectors. Now, if we restrict our attention to lightly absorbing crystals we can write

$$\begin{aligned}R_0=(c/8\pi)\gamma_0\left[\int_T^R|\Sigma\varphi_0^{(j)}|^2d\tau+\int_{\varepsilon_1}\{|\Phi_c|^2-|\Phi_s|^2\}d\tau\right]\\ =R_0'+R_0''\end{aligned} \qquad (62)$$

in deriving this, ε_2 is replaced by $\varepsilon_1+\varepsilon_2$ in R_0'. This approximation is justified since ε_1 is very small and $|\Sigma\varphi_0^{(j)}|$ has a finite value in ε_1. Calculation shows that

$$R_0'=-(R_g-\alpha\beta t_0 I_e) . \qquad (63)$$

(See Appendix B). Therefore, if we postulate that

$$R_0+R_g=0 , \qquad (64)$$

which condition applies as long as absorption is low enough for the Borrmann effect to be neglected, we can conclude that

$$R_0''=-I_e(\alpha\beta t_0) , \qquad (65)$$

which quantity is in fact the negative of the integrated intensity based upon the kinematical theory. This result is reasonable because a transmitted beam travelling towards the ε_1-region should lose some energy due to single scattering by an amount which must be predicted by the kinematical theory. Thus, we can interpret $|\Sigma\varphi_0^{(j)}|^2$ as that part of the transmitted beam due to multiple reflection.

7. Discussion and conclusions

It is a characteristic feature of 'Pendellösung' phenomena in X-rays that there exists a phase relation among different parts of the incident wave which propagate in different directions. This relation is significant in single-crystal experiments concerned with spatial intensity distributions but not with measurements of integrated intensities.

Energy-flow theories (Laue, 1952; Kato, 1958, 1960) cannot predict such interference phenomena properly since this approach excludes consideration of coherence between different flows. The wave-bundle approach (Ewald, 1958; Kato, 1952, Part 1) and the spherical-wave theory (Part 2) which is actually a more explicit but special treatment of the wave bundle approach, are necessary for understanding these phenomena. As pointed out in Section 4, the present approach can predict the same results as can energy-flow theories with respect to the limitation of appreciable wave fields within the area included between $\mathbf{K}_B$ and $\mathbf{K}_B+2\pi\mathbf{g}$.

We must distinguish the essential difference of diffraction phenomena between electron and X-ray cases (Part 1). Similarity of electron micrographs and the traverse patterns of X-rays is only superficial. Nevertheless, the electron theory can be applied to X-ray cases if we use it with proper caution. Particularly, from a practical viewpoint, it is very convenient to use it in calculating fringe spacings of the traverse pattern of thicker parts of a crystal, just as shown in the previous paper (Kato & Lang, 1959). The electron theory shows a clear geometrical picture of the relations between the wave vectors and the crystal surface. It should be noticed that we will obtain the same patterns as an X-ray traverse pattern in an electron micrograph if we use an incident beam of wide angular range with no phase relationships.

In thin parts of a crystal, the steepest-descent approach or the wave-bundle approach is not applicable since the Fraunhofer condition in a crystalline medium (Part 1) does not hold in such parts. Thus, we can expect a contraction of the first few fringe spacings due to the form of Bessel functions. It seems, however, that the magnitude of contraction is not enogh to explain a small discrepancy between the

plane wave theory and the experiments which is pointed out in the earlier paper (Kato & Lang, 1959). In the R and r net planes of quartz we always observed about 10 fringes, so that we cannot in this case expect any discrepancy. In other cases, we would not expect a discrepancy of more than about 1%, which is comparable with experimental errors. Rather careful studies on absorption effects (Section 4) also cannot explain the discrepancy. We have to leave this problem as unsolved.

APPENDIX A

The wave fields of non-absorbing crystals have the form

$$\Sigma\varphi_0^{(j)}=K_0U_0 \quad \text{and} \quad \Sigma\varphi_g^{(j)}=K_gU_g\,, \qquad \text{(A-1)}$$

where K_0 and K_g are constants and

$$U_0=\int_{-\infty}^{+\infty}\{(-s+(s^2+\beta^2)^{\frac{1}{2}})\exp[i\alpha t_0(s^2+\beta^2)^{\frac{1}{2}}] +(s+(s^2+\beta^2)^{\frac{1}{2}})\exp[-i\alpha t_0(s^2+\beta^2)^{\frac{1}{2}}]\} \times\exp[-iqt_0s]/(s^2+\beta^2)^{\frac{1}{2}}\,ds \qquad \text{(A-2)}$$

$$U_g=\int_{-\infty}^{+\infty}\{\exp[i\alpha t_0(s^2+\beta^2)^{\frac{1}{2}}]-\exp[-i\alpha t_0(s^2+\beta^2)^{\frac{1}{2}}]\} \times(\exp -iqt_0s)/(s^2+\beta^2)^{\frac{1}{2}}\,. \qquad \text{(A-3)}$$

By means of a well-known Fourier transform (see Sneddon, 1951) we may express (A-3) as

$$\begin{aligned} U_g &= 2\pi i J_0(\beta t_0(\alpha^2-q^2)^{\frac{1}{2}}) && |q|<|\alpha| \\ &= 0 && |q|>|\alpha|\,. \end{aligned} \qquad \text{(A-4)}$$

If we notice a relation between U_0 and U_g through their integrand of the form

$$U_0=\partial U_g/\partial(iqt_0)+\partial U_g/\partial(i\alpha t_0)$$

we can easily obtain

$$\begin{aligned} U_0 &= 2\pi\beta\{(\alpha-q)/(\alpha+q)\}^{\frac{1}{2}}J_1(\beta t_0(\alpha^2-q^2)^{\frac{1}{2}}) && |q|<|\alpha| \\ &= 0 && |q|>|\alpha|\,. \end{aligned} \qquad \text{(A-5)}$$

APPENDIX B

Integrations necessary for the integrated intensities are

$$R_0'=\frac{\pi}{2}I_e d\int_a^b\frac{b-\tau}{\tau-a}J_1^2(\zeta)\,d\tau \qquad \text{(B-1)}$$

and

$$R_g=\frac{\pi}{2}I_e d\int_a^b J_0^2(\zeta)\,d\tau\,, \qquad \text{(B-2)}$$

where ζ is given by equation (54) and

$$d=K|\psi_g^r|\sin\chi(\gamma_0\gamma_g)^{\frac{1}{2}}/(\sin 2\theta_B). \qquad \text{(B-3)}$$

Using Neumann's series for the square of a Bessel function (see Watson, 1944)

$$J_n^2(\zeta)=\frac{(\frac{1}{2}\zeta)^{2n}}{(n!)^2}\left\{1-\frac{T_2\zeta^2}{1.(2n+1)}+\frac{T_4\zeta^4}{1.2(2n+1)(2n+2)}+\cdots\right\},$$

where

$$T_2=\frac{2n+1}{2n+2},\quad T_4=\frac{(2n+1)(2n+3)}{(2n+2)(2n+4)}\cdots,$$

we can show that

$$R_0'=\frac{\pi}{2}I_e\int_a^b\left(\frac{b-\tau}{\tau-a}\right)\sum_{m=0}^{\infty}a_{2m}d^{2m+3}(b-\tau)^{m+1}(\tau-a)^{m+1}d\tau$$

and $\qquad \text{(B-4)}$

$$R_g=\frac{\pi}{2}I_e\int_a^b\sum_{m=0}^{\infty}b_{2m}d^{2m+1}(b-\tau)^m(\tau-a)^m d\tau\,, \qquad \text{(B-5)}$$

where

$$a_{2m}=(-)^m\frac{1}{m!(m+2)!}\frac{(2m+1)!!}{(2m+2)!!} \qquad \text{(B-6)}$$

and

$$b_{2m}=(-)^m\frac{1}{(m!)^2}\frac{(2m-1)!!}{2m!!} \qquad \text{(B-7)}$$

If we make the substitution

$$\frac{\tau-a}{b-\tau}=u$$

the integrations are reduced to the following type:

$$\int_0^{\infty}\frac{u^{p-1}}{(1+u)^{p+q}}du=\frac{\Gamma(p)\Gamma(q)}{\Gamma(p+q)}.$$

Moreover,

$$d(b-a)=2\alpha\beta t_0\,. \qquad \text{(B-8)}$$

This is equal to the quantity $2A$ in Zachariasen's notation, and πA can be interpreted as an integrated intensity due to a single scattering (Zachariasen, 1945). Thus, we can show that

$$R_0'=-\frac{\pi}{2}I_e\sum_{m=1}^{\infty}(-)^m\frac{1}{(2m+1)!}\frac{(2m-1)!!}{2m!!}(2\alpha\beta t_0)^{2m+1} \qquad \text{(B-9)}$$

$$R_g=\frac{\pi}{2}I_e\sum_{m=0}^{\infty}(-)^m\frac{1}{(2m+1)!}\frac{(2m-1)!!}{(2m)!!}(2\alpha\beta t_0)^{2m+1} \qquad \text{(B-10)}$$

$$=\frac{\pi}{2}I_e\int_0^{2\alpha\beta t_0}J_0(\varrho)\,d\varrho\,. \qquad \text{(B-11)}$$

The author wishes to express his thanks to the Office of Naval Research for the financial support that enabled this study to be undertaken. He wishes also to express his great thanks to Prof. P. P. Ewald for his kind and valuable discussion and to Prof. A. R. Lang for his encouragement and discussion in preparing this paper.

References

EWALD, P. P. (1958). *Acta Cryst.* **11**, 887.
JEFFREYS, H. & JEFFREYS, B. S. (1946). *Method of*

Mathematical Physics, chapter 17. Cambridge: Univ. Press.
KATO, N. (1952). *J. Phys. Soc. Jap.* **7**, 397.
KATO, N. (1955). *J. Phys. Soc. Jap.* **10**, 46.
KATO, N. (1958). *Acta Cryst.* **11**, 885.
KATO, N. (1960). *Acta Cryst.* **13**, 349.
KATO, N. & LANG, A. R. (1959). *Acta Cryst.* **12**, 787.
LAUE, M. v. (1952). *Acta Cryst.* **5**, 619.
SNEDDON, I. N. (1951). *Fourier Transforms*, Table II. New York: McGraw-Hill.
WALLER, I. (1926). *Ann. Phys.* **79**, 261.
WATSON, G. N. (1944). *A Treatise on the Theory of Bessel Functions*, p. 32. Cambridge: Univ. Press.
ZACHARIASEN, W. H. (1945). *Theory of X-ray Diffraction in Crystals*, Section III, p. 8. New York: Wiley.

Acta Cryst. (1961). **14**, 636

Orientated Crystal Growth in Electrodeposits, in Relation to Ionic Diffusion in the Electrolyte

BY H. I. MATTHEWS, T. DE S. MUTUCUMARANA AND H. WILMAN

Applied Physical Chemistry of Surfaces Laboratory, Chemical Engineering Department, Imperial College, London, S.W. 7, England

(*Received* 26 *July* 1960)

The structure and form of dendritic Cu and Ag electrodeposits from $CuSo_4$ and $AgNO_3$ solution are studied as a function of the current density (i) and time of deposition (t), by means of light microscopy, electron microscopy and electron diffraction. The structure and orientation are considered particularly in relation to the time τ of deposition giving first visible dimming of an initially smooth cathode ($i\sqrt{\tau}=$constant), and also in relation to the observed crystal habit. The micrographs show that the crystals have pronounced {111} faces parallel to the plane of the stems and branches of the dendrites. This is associated with a preferred orientation of the deposit with a ⟨110⟩ direction normal to the cathode, although in several cases ⟨210⟩ orientation was developed. The details of the electron micrographs indicate that the dendrites arise from the pronounced preferential deposition of cations on projecting parts of the cathode owing to their motion being limited by diffusion. This diffusion effect also accounts for the variation, with current density, of the deposit thickness at which twinning develops, in the results of Setty & Wilman (1955).

1. Introduction

Electron-diffraction experiments in this laboratory (Finch & Sun, 1936; Finch & Williams, 1937) showed that metal electrodeposits at low current densities tend to grow as crystals having the most densely populated atomic plane parallel to the substrate ('lateral growth'). Those formed at higher current densities tend to develop a preferred crystal orientation with the most densely populated lattice row normal to the substrate ('outward growth').

Finch, Wilman & Yang (1947) have shown that, even in the 'lateral' type of growth on a smooth electropolished substrate, preferential deposition on small projections of the cathode surface occurs and leads to progressive roughening of the deposit surface. Furthermore, it was concluded that 'outward growth', with its characteristic preferred orientation, was due to this tendency, and was favoured by low bath temperature, low concentration of the electrolyte, high current density, and absence of stirring. All these features indicate that such growth is due to the rapid impoverishment of the solution near the cathode, with respect to the cations, and the slowness of their replacement by diffusion from regions of solution further away from the cathode. Under conditions very strongly favouring outward growth, the deposits develop as needle-shaped or dendritic crystals having the above characteristic orientation (Finch & Layton, 1951).

In view of the present importance of such deposits for preparation of powders suitable for use in powder metallurgy, we have now examined this 'outward' type of cathodic crystal growth in more detail in the case of copper and silver. The results, described below, are considered in relation to the published results on the change in cation concentration near the cathode as deposition proceeds, and the related stage of visual dimming or roughening of the cathode, which is observed after a time τ of deposition given by $i\sqrt{\tau}=$ constant (Ullman, 1897; Sand, 1900, 1901; Sebborn, 1933; Kudra, 1934, 1935, 1936, 1937, 1938*a*, *b*; Kaneko & Kawamura, 1940; Wranglen, 1950; Ibl & Trümpler, 1952, 1953; Modi & Tendolkar, 1953; Ibl 1954).

2. Experimental

Electrodeposits were prepared from 0·1 and 0·3*M* $CuSO_4$ and 0·1*M* $AgNO_3$ solutions in water, about